Lipid domains control myelin basic protein adsorption and membrane interactions between model myelin lipid bilayers

Dong Woog Lee[a], Xavier Banquy[a,b], Kai Kristiansen[a], Yair Kaufman[a], Joan M. Boggs[c,d], and Jacob N. Israelachvili[a,e,1]

[a]Department of Chemical Engineering, University of California, Santa Barbara, CA 93106; [b]Faculty of Pharmacy, Université de Montréal, Montréal, QC, Canada H3C 3J7; [c]Department of Molecular Structure and Function, The Hospital for Sick Children, Toronto, ON, Canada M5G 1X8; [d]Department of Laboratory Medicine and Pathobiology, University of Toronto, Toronto, ON, Canada M5G 1L5; and [e]Materials Department, University of California, Santa Barbara, CA 93106

Contributed by Jacob N. Israelachvili, January 21, 2014 (sent for review October 4, 2013)

The surface forces apparatus and atomic force microscope were used to study the effects of lipid composition and concentrations of myelin basic protein (MBP) on the structure of model lipid bilayers, as well as the interaction forces and adhesion between them. The lipid bilayers had a lipid composition characteristic of the cytoplasmic leaflets of myelin from "normal" (healthy) and "disease-like" [experimental allergic encephalomyelitis (EAE)] animals. They showed significant differences in the adsorption mechanism of MBP. MBP adsorbs on normal bilayers to form a compact film (3–4 nm) with strong intermembrane adhesion (~0.36 mJ/m^2), in contrast to its formation of thicker (7–8 nm) swelled films with weaker intermembrane adhesion (~0.13 mJ/m^2) on EAE bilayers. MBP preferentially adsorbs to liquid-disordered submicron domains within the lipid membranes, attributed to hydrophobic attractions. These results show a direct connection between the lipid composition of membranes and membrane–protein adsorption mechanisms that affects intermembrane spacing and adhesion and has direct implications for demyelinating diseases.

lipid raft | biomembrane adhesion | myelin structure | multiple sclerosis | intrinsically unstructured proteins

Myelin is an asymmetric multilamellar membrane wrapped around the axons of the central nervous system (CNS) and consists of alternating extracellular and cytoplasmic leaflets (1–3). The bilayer-associated proteins, mainly myelin basic protein (MBP) and proteolipid protein, play an essential role in stabilizing and maintaining the myelin structure. The bilayers are in close contact (~3 nm separation between lipid headgroup–water interfaces), providing a low dielectric constant through the compact bilayers, which is essential for efficient and fast saltatory propagation of nerve impulses. Any structural changes of the myelin sheath in the CNS, including lesion formation, loss of adhesion, swelling of the water gaps, vacuolization, vesiculation, and complete delamination (demyelination) of the myelin sheath (4–6), are signatures of several inflammatory neurological disorders. These types of disorders are characterized by a broad spectrum of neurological symptoms, such as physical and cognitive disabilities, with multiple sclerosis (MS) being one of the most common demyelinating diseases (2).

The primary cause of structural changes in the myelin is still under debate; however, morphological changes of the myelin structure due to diseases such as MS are well known. A well-studied and accepted animal model for MS is the experimental allergic encephalomyelitis (EAE) of the marmoset (2, 6). Using this model, recent studies conducted with the surface forces apparatus (SFA) have shown that a loss of adhesion force (7) and structural changes of model membranes with lipid composition characteristic of myelin accompanied compositional alterations of the lipid species (8), as well as an electric charge imbalance between lipid molecules and MBP (9). These alterations also change the lateral distribution and stability of phase-separated lipid domains (or rafts) within model myelin membranes (8, 10).

MBP is one of the most abundant proteins in the CNS and is an intrinsically unstructured (disordered) protein (11). MBP acts as an intermembrane adhesion protein between the cytoplasmic leaflets of the myelin sheath. The predominant size and charge isoform of MBP in healthy and mature myelin has a molecular weight of 18.5 kDa and a net positive charge of 19 (12, 13). Several studies conducted with model and extracted myelin bilayers (9, 14–19) showed that because of its high content of positively charged residues, MBP binds to the negatively charged lipids of the cytoplasmic leaflets of the bilayer via electrostatic interaction in addition to hydrophobic interactions. However, studies have shown that the MBP charge component composition, as well as the balance between charged lipids and MBP charge components, changes in EAE (as well as in MS) tissues (20, 21). Other studies (9, 15) demonstrated the importance of the hydrophobic interaction between MBP and lipid membranes by showing that MBP specifically binds to lipid domain boundaries (defects), altering the lateral organization of the model myelin bilayers. A recent study also showed that MBP's association with the cytoplasmic leaflet of the myelin membrane induces a phase transition into a cohesive mesh-like protein network (22, 23).

Significance

The proper functioning of multilayer membrane systems, such as myelin, requires the multilamellar membranes to be tightly wrapped around the axon fibers, thereby allowing efficient electric signal transmission. Slight changes in lipid composition in myelin membranes will alter their domain sizes and distributions, and the intermembrane adhesive properties. Using the surface forces apparatus and atomic force microscope, we studied the adsorption of myelin basic protein (MBP) to model myelin lipid bilayer membranes of varying compositions, and their effects on the structure, equilibrium spacing (swelling), and adhesion force between them. We find that MBP preferentially adsorbs to "disordered" submicron domains, affecting regular spacing and adhesion. These findings provide insights into lipid–protein interactions and membrane-associated (e.g., demyelinating) diseases.

Author contributions: D.W.L. designed research; D.W.L., X.B., K.K., and Y.K. performed research; D.W.L. analyzed data; and D.W.L., X.B., K.K., Y.K., J.M.B., and J.N.I. wrote the paper.

The authors declare no conflict of interest.

Freely available online through the PNAS open access option.

[1]To whom correspondence should be addressed. E-mail: jacob@engineering.ucsb.edu.

This article contains supporting information online at www.pnas.org/lookup/suppl/doi:10.1073/pnas.1401165111/-/DCSupplemental.

One open question regarding the stability of myelin membranes is how the concentration of MBP affects the interaction forces between myelin bilayers. We reconstructed and used two types of supported model monolayers with a lipid composition characteristic of "normal" or "healthy" and "disease-like" EAE myelin deposited on a dipalmitoylphosphatidylethanolamine (DPPE) monolayer to examine the effect of lipid composition, domains, and fluidity on the interaction forces, film viscosity, and MBP adsorption mechanism between these model myelin bilayers. The lipid composition used is based on data from Inouye and Kirschner (1, 24) and Ohler et al. (6) (Table 1). For convenience, these reconstituted bilayers are referred to as "model normal bilayers," "model EAE bilayers," and "model myelin bilayers" throughout this article. The bilayers were prepared using the Langmuir–Blodgett technique (25), and the interaction forces were measured using surface forces apparatus (SFA) model 2000 (26), with the capacity of measuring interaction forces and separation distances between macroscopic surfaces with a resolution of 10 nN and 0.1 nm, respectively. The MBP adsorption mechanism onto the bilayers also was examined using an atomic force microscope (AFM). This study aims to establish the relationship between the structure of the model lipid myelin bilayers and protein adsorption and also to quantify the effect of MBP concentration on the intermembrane interaction forces.

Results

Interaction Forces Between Supported Model Cytoplasmic Myelin Bilayers. MBP is a flexible, elongated biomolecule (11) that contains both charged and hydrophobic/hydrophilic groups and interacts readily with lipid bilayers. The adhesive strength and density of an ensemble of MBPs between myelin lipid bilayers, obtained through force–distance (*F–D*) and thin-film viscosity measurements (see Fig. 1 for a schematic of the experimental setup), provided qualitative and quantitative information about the interfacial MBP conformation and adsorption mechanism at the molecular level.

Force–distance profiles show there is a critical adsorption concentration, C_{crit}, of MBP above which MBP adsorbs (Fig. 2). This adsorption threshold is a characteristic feature of domain formations of molecules (2D micelles, clusters, or rafts) (27). At bulk concentrations C of MBP that are less than 1.2 ng/mL, the MBP adsorbs to neither normal (Fig. 2 *A–C*) nor EAE (Fig. 2 *D–F*) model myelin bilayers and the bilayer's interactions are similar to two bare bilayers. When the MBP concentration exceeds 2.9 ng/mL, rapid and cooperative adsorption of MBP occurs, as may be ascertained from the following observations (Fig. 2): (*i*) Over a slight increase in the MBP concentration, a sharp outward shift of the electric double-layer interaction and the steric "hard wall" ($D_{sw} = 2D_B + D_{MBP}$ at $F/R \sim 4$ mN/m) from $D_{sw} \sim 10$ nm (corresponding to two bilayers in contact, $D_B = 5$ nm and $D_{MBP} = 0$ nm) to $D_{sw} \sim 13$ nm (two normal bilayers plus one layer of MBP, $D_B = 5$ nm and $D_{MBP} = 3$ nm) or $D_{sw} \sim 17$ nm (two EAE bilayers plus a swollen layer of MBP, $D_B = 5$ nm and $D_{MBP} = 7$ nm) is observed. (*ii*) The adhesion (pull-off) force increases concomitantly with the adsorption of MBP, as measured on separation.

Table 1. Lipid compositions used for the reconstituted cytoplasmic myelin lipid monolayers

	Mole % lipid	
Lipid class	Normal	EAE
Cholesterol	31.6	37.4
PS^{-}	7.3	7.4
$SM^{+/-}$	6.2	2.2
$PC^{+/-}$	25.9	20.1
$PE^{+/-}$	29.0	32.9

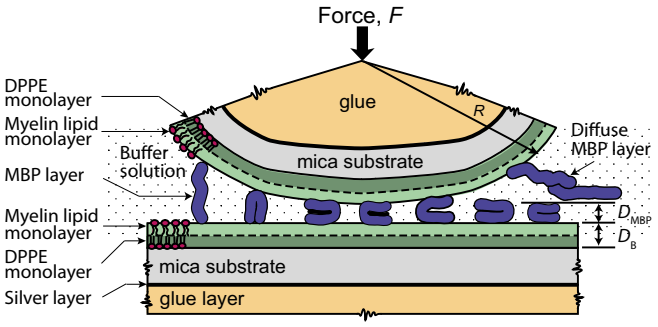

Fig. 1. Schematic representation of the model myelin bilayer system. Two apposing model myelin bilayers deposited on solid mica substrates were immersed in an aqueous buffer solution (saturated with lipids) with a bulk MBP concentration of *C*. By using the Langmuir–Blodgett technique, a DPPE monolayer was deposited as the supporting layer on atomically smooth mica. The myelin (cytoplasmic leaflet) lipid monolayer was deposited above the predeposited DPPE monolayer. To adsorb MBP to the bilayer surfaces, the MBP solution (in sodium nitrate buffer) was injected into the medium with a syringe after separating two bilayers far from each other ($D > 1$ mm). An equilibration time of 30 min was used after every injection.

Intermembrane distances and adhesion are important parameters for how well a myelin membrane functions. A low intermembrane distance within the multilayer myelin membrane gives a lower dielectric constant between the core axon and the surrounding medium and, according to cable theory, a faster transition time of nervous signal through the axon, compared with a swelled membrane (9). Fig. 3 shows the normalized adhesion force F_{ad}/R ($= \min[F/R]$), adhesion energy per unit area E_{ad} [$= -2F_{ad}/3\pi R$, the Johnson, Kendall, and Roberts (JKR) model (28, 29)], steric hard-wall thickness D_{sw}, and jump-from distance D_j measured by the SFA, as a function of bulk MBP concentration C. As shown in Fig. 3*A*, the increase of F_{ad}/R with C is abrupt and large ($F_{ad}/R \sim -1.7$ mN/m, $E_{ad} \sim 0.36$ mJ/m^2) in the normal bilayer, whereas in the EAE bilayer, the F_{ad}/R increase is rather gradual and smaller ($F_{ad}/R \sim -0.6$ mN/m, $E_{ad} \sim 0.13$ mJ/m^2). As shown in Fig. 3*B*, the comparison of D_{sw} clearly shows that model EAE bilayers exhibit a swollen layer of MBP ($D_{MBP} \sim 7$–8 nm) at $C > 2.9$ ng/mL, whereas D_{MBP} in the normal bilayer is compact, with a thickness equal to that of a single MBP molecule, σ_{MBP} ($D_{MBP} \sim 3$–4 nm) as measured by electron microscopy, X-ray, and computational techniques (14, 30, 31). Following the same trend, D_j is larger in the EAE bilayer (Fig. 3*C*), which is a possible indication of the formation of a thicker gel-like layer on EAE bilayers at $C > 5.8$ ng/mL. Structural changes (e.g., swelling, lesion formations) in autoimmune diseases such as EAE and MS have been observed in the extracellular leaflet of myelin membranes in the CNS only, by using electron microscopy (4, 6). Other studies have reported an alteration in the MBP composition and concentration in the cytoplasmic leaflet (12, 20). Fig. 3 clearly shows that both the adhesion energy between (model) cytoplasmic leaflets and the intermembrane distance are sensitive to MBP concentration. Any out-of-balance concentration of MBP likely will result in some instability in myelin structure and greater access of anti-MBP T cells and/or antibodies to MBP at the cytoplasmic leaflet, possibly after some degree of breakdown of myelin due to other factors.

The differences in adhesion and MBP layer thickness between normal and EAE bilayers demonstrate the sensitivity of these properties to subtle changes in lipid composition (Table 1), which is related to fluidity and lipid domain distributions (8, 10). These changes in lipid membrane fluidity and domain structures

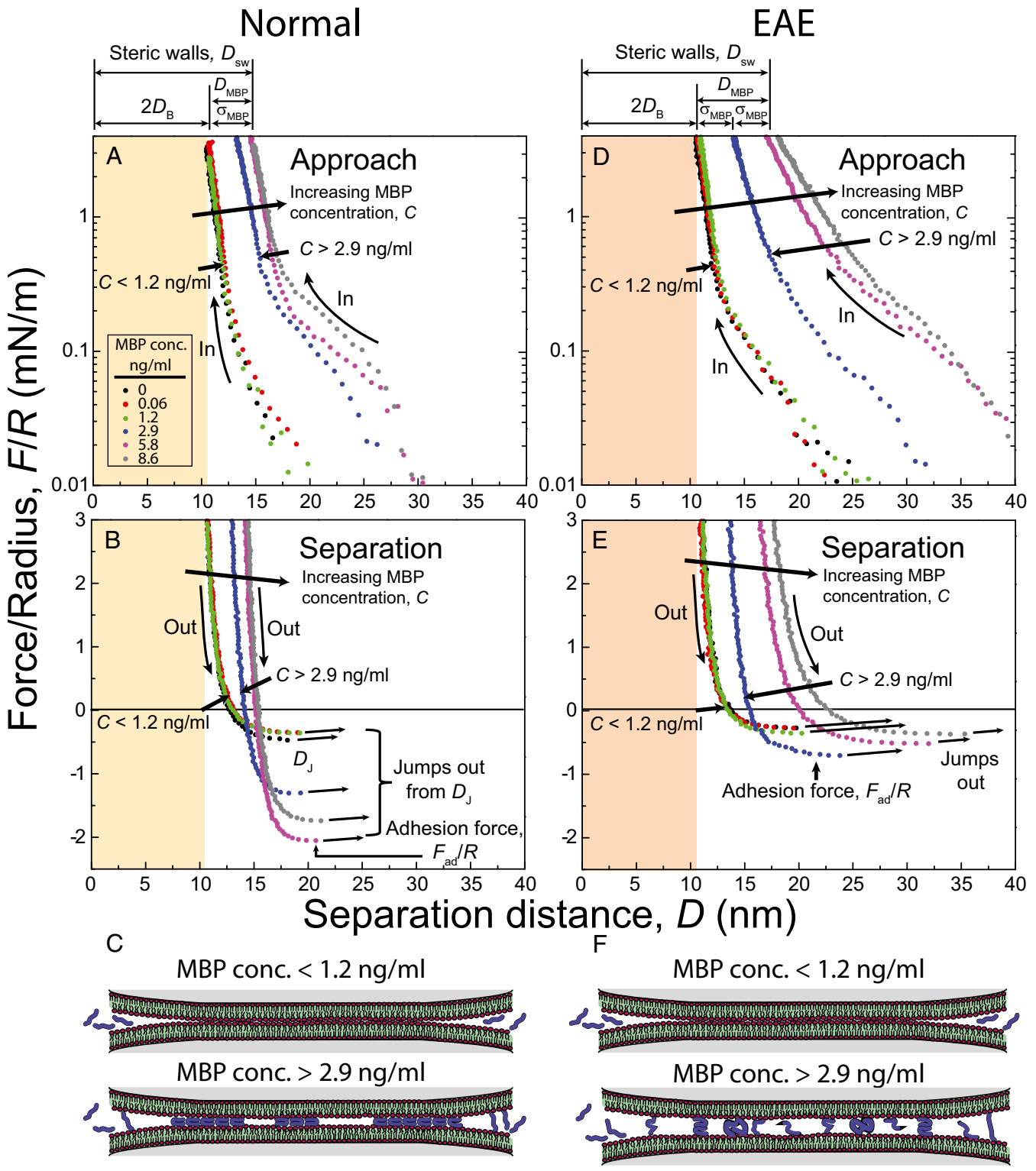

Fig. 2. Normalized force–distance profiles measured at different MBP concentrations *C* and schematics of both the normal (*A*–*C*) and EAE (*D*–*F*) bilayers. The normal force *F* is measured between two cylindrical surfaces of radius *R*, as a function of the separation distance *D* (*D* = 0 at mica–mica contact in air). D_B, D_{sw}, D_{MBP}, D_j, and σ_{MBP} indicate bilayer thickness, steric wall thickness, MBP film thickness, "jump-from" distance, and size of a single MBP, respectively.

may cause abnormal adsorption and/or conformations of MBP, which might make myelin less stable and more susceptible to attack by the immune system, allowing its eventual disintegration. MBP then might be exposed to proteolytic degradation and release of immunogenic epitopes, which also contribute to demyelination (21).

The surface concentration of MBP (Γ, mass per unit area) adsorbed onto the bilayer is directly related to the normalized

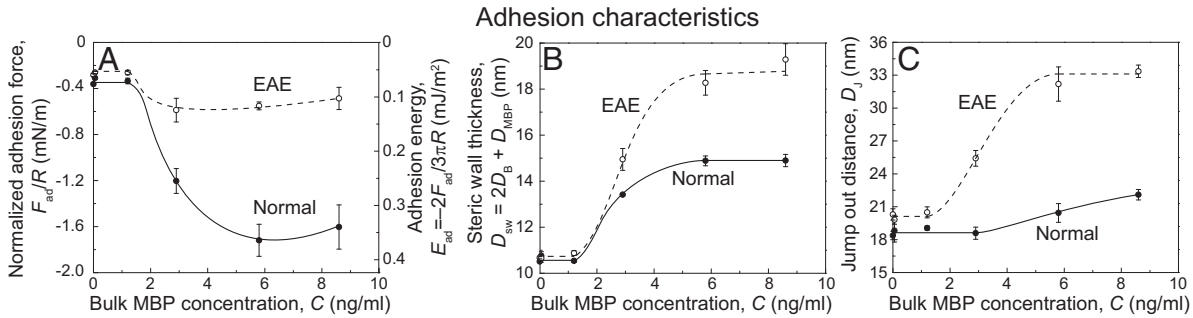

Fig. 3. Measured parameters from the force–distance profiles in Fig. 2. (*A*) Normalized adhesion force, F_{ad}/R, and adhesion energy, E_{ad}; (*B*) steric wall thickness, D_{sw}; and (*C*) jump-out distance, D_j, are plotted as a function of bulk MBP concentration *C*. Above C_{crit}, with increasing concentration, the adhesion force increases up to a certain *C*; however, the adhesion force of the normal bilayer was significantly higher while maintaining a more compact structure compared with the EAE bilayer. Error bars indicate SD of more than five different replicates.

adhesion force F_{ad}/R (Fig. 4). The surface concentration is calculated (Fig. 4*A*) by the refractive index n of the medium (including MBP, water, and lipids) measured by using an optical technique with the SFA (32). The volume fraction of MBP in the adsorbed film, ϕ_{MBP}, is calculated based on the following equation (33):

$$n^2(D) = n_B^2\phi_B^2 + n_{MBP}^2\phi_{MBP}^2 + n_w^2\phi_w^2,\ \phi_B + \phi_{MBP} + \phi_w = 1, \quad [1]$$

where $n(D)$ is the measured refractive index, n_x is a refractive index of component x, and ϕ_x is a volume fraction of component x, where the subscripts B and w indicate lipid bilayer and water, respectively. The value of n_B is approximated as the measured refractive index at $D = 2D_B$ without MBP present in the solution. The values of n_{MBP} and n_w are 1.55 (34, 35) and 1.33, respectively. The surface concentration of MBP, Γ, is obtained using the following equation (Fig. 4*B*) (36):

$$\Gamma = 0.5 \cdot \rho_{MBP} \cdot D \cdot \phi_{MBP}, \quad [2]$$

using an MBP density ρ_{MBP} of 1.38 g/cm^3 (37). Finally, the calculated values of Γ may be correlated directly to the measured normalized adhesion force F_{ad}/R.

Fig. 4*C* shows that the magnitude of F_{ad}/R increases linearly with Γ for both the normal and EAE bilayers up to a certain level ($\Gamma = \Gamma_{max}$) and reaches a plateau or slightly decreases afterward. This effect may be the result of a charge reversal (positive charges of MBP overwhelm the negative charges of both lipid bilayers) or gelation (9) from the dominance of intermolecular cohesion of MBP rather than the adhesion between the MBP and bilayers.

The MBP adsorption mechanism determines the MBP conformation between the surfaces and therefore the intermembrane adhesion. The "optimal" amount of MBP adsorbed at the myelin membrane coincides with the maximum value of F_{ad}/R (Fig. 4): at maximum values of F_{ad}/R of 2 mN/m and 0.6 mN/m, the MBP surface concentrations Γ_{max} are 1.8 and 2.5 mg/m^2 for normal and EAE bilayers, respectively (Fig. 4*C*). Assuming that only a certain fraction of MBP, ξ, on the bilayers is participating in the adhesion, the adhesion energy per MBP molecule E_{MBP} may be estimated using the JKR model for soft materials with large deformations (28, 29), $E_{ad} = -2F_{ad}/3\pi R$ (maximum "total" adhesion energy per unit area), and the following equation:

$$E_{MBP} = \frac{E_{ad}}{\xi\Gamma_{max}} = -\frac{2F_{ad}}{3\pi R\xi\Gamma_{max}}. \quad [3]$$

The adhesion energy per MBP molecule was calculated as $E_{MBP} = 1.7/\xi$ kT (energy unit) for normal and $0.3/\xi$ kT for EAE, respectively. MBP with the right conformation for interbilayer adhesion should have the same E_{MBP}. Assuming that the magnitudes of the binding energy per molecule of the normal and EAE membranes are similar, we infer that the ξ value of a normal myelin bilayer is approximately six times higher than that of an EAE myelin bilayer.

The ξ value depends on many factors, such as the contact time during the force–distance measurements, rate of separation, temperature, and adsorption mechanism. Because all other factors were maintained constant, we conclude that the difference of ξ between the normal and EAE myelin bilayers emerges from the different mechanisms of MBP adsorption, causing conformational and orientational differences in MBP. Also, the different MBP

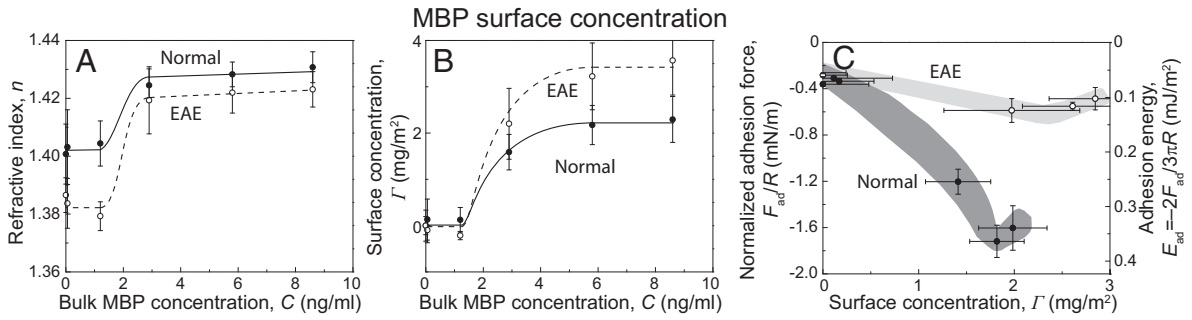

Fig. 4. Calculated parameters from analyzing the fringes of equal chromatic order images. (*A*) Refractive index, *n*, and (*B*) surface concentration, Γ, are plotted as a function of bulk MBP concentration *C*. (*C*) F_{ad}/R is plotted as a function of Γ. The normal bilayer exhibits higher F_{ad}/R at every Γ, indicating that the structure and/or orientation of MBP adsorbed on the normal bilayer are different from those of MBP on the EAE bilayer, and more optimized for interbilayer adhesion compared with the EAE bilayer. Error bars indicate the propagated error from the values measured in Fig. 3.

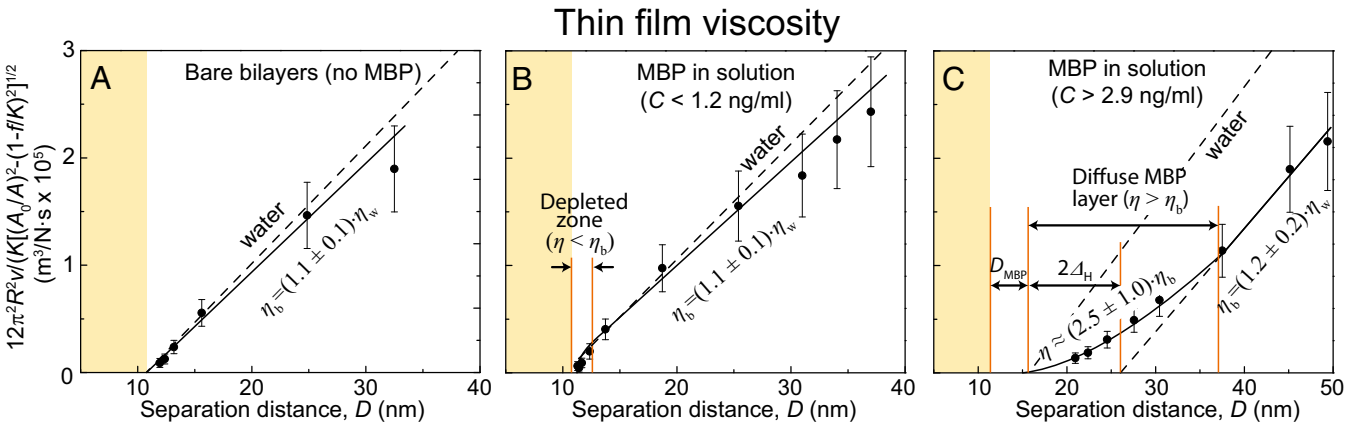

Fig. 5. Plots of viscosity measurements performed between EAE bilayers measured at different MBP concentrations: (*A*) C = 0 ng/mL, (*B*) 0 < C < 1.2 ng/mL, and (*C*) C > 2.9 ng/mL. The inverse of the slope represents the film viscosity. The dashed line indicates water viscosity at 24 °C, which is 0.91 mPa/s.

adsorption mechanisms mainly are a result of the difference in the lipid compositions and fluidity.

MBP Film Viscosity Between Supported Cytoplasmic Model Myelin Bilayers. The thin film rheology measurement between the model myelin bilayers provides information about the thin film viscosity, η; hydrodynamic thickness, Δ_H; and diffuse layer thickness (38, 39) of MBP. The thin film rheology study measures the coupling between oscillation (vibration) of the upper cylindrical surface (amplitude A_o and frequency v) in the z-direction with a lower surface that is suspended on a cantilever spring with spring stiffness K (38) (see *Materials and Methods* for details). When the separation distance D between the two apposing surfaces is large, the lower surface does not move because of weak viscous coupling between the two surfaces. As D is reduced gradually while the upper surface is oscillated, the lower surface starts to "feel" the viscous force induced by the oscillation of the upper surface and oscillates at a relative amplitude A. When D approaches D_{sw}, all the energy generated from the oscillation of the upper surface is transmitted to the lower surface without any energy loss, causing the two surfaces to move in phase with $A = 0$. The relation between viscosity, η; the distance between two surfaces, D; the applied

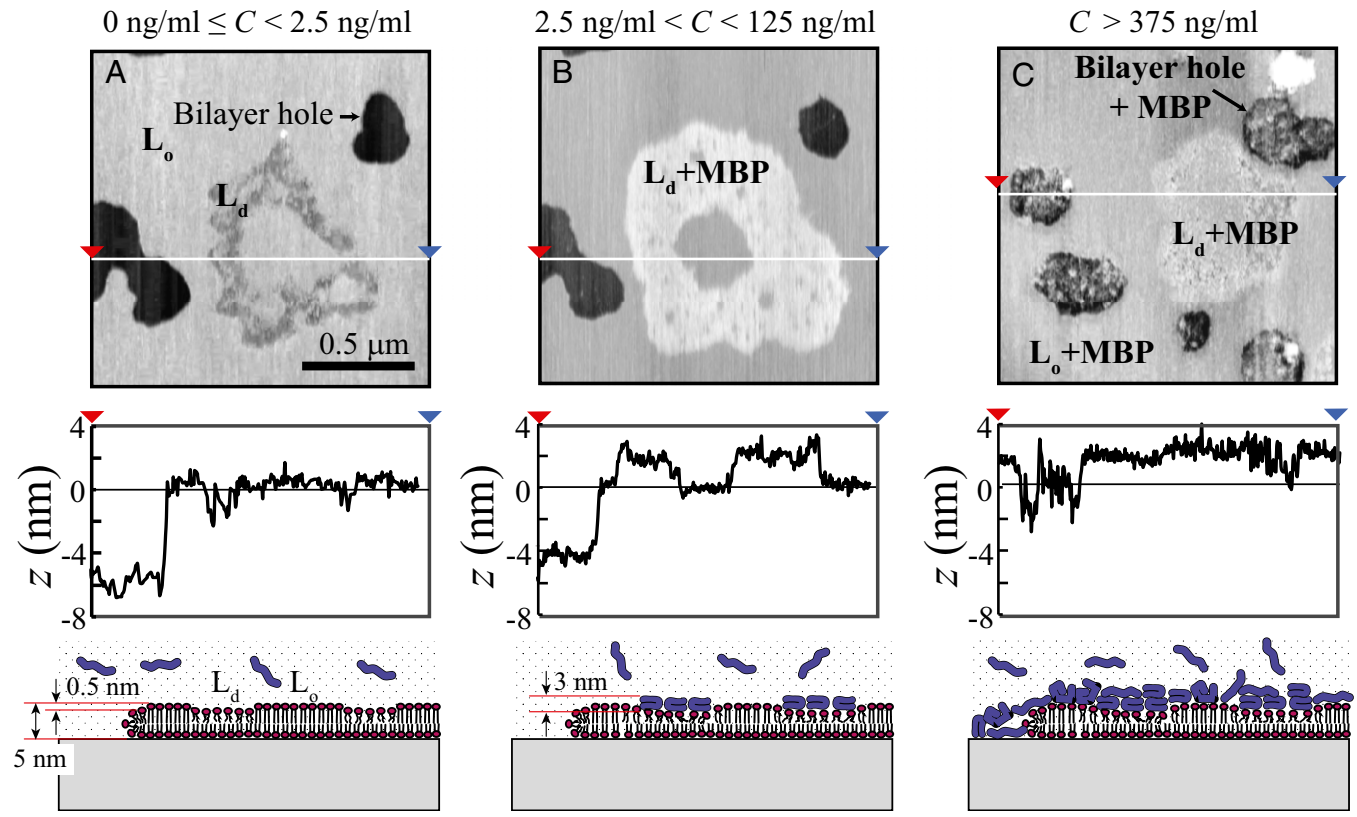

Fig. 6. AFM images of EAE model myelin bilayers at an MBP concentration C of (*A*) C < 2.5 ng/mL, (*B*) 2.5 ng/mL < C < 125 ng/mL, and (*C*) C > 375 ng/mL. Bilayer holes occupy less than 14% in area fraction. AFM images *A* and *B* are the same area. Lipid domains are observed in EAE lipid bilayers. The height difference (Δz) between L_o and L_d phase was ~0.5 nm.

vibration frequency, v; the applied vibration amplitude, A_o; and the measured relative amplitude A is expressed as (38)

$$\eta(D) = \frac{KD}{12\pi^2 R^2 v}\left[\left(\frac{A_o}{A}\right)^2 - \left(1-\frac{f}{K}\right)^2\right]^{1/2}, \quad [4]$$

where $f = dF(D)/dD$ is the gradient of the interfacial force.

Fig. 5 shows plots of $12\pi^2R^2v/(K[(A_0/A)^2-(1-f/K)^2]^{1/2})$ against D measured between EAE bilayers, where the inverse slope of the plotted line gives the viscosity. When the bulk concentration, C, of MBP is less than 1.2 ng/mL (Fig. 5*B*), no signs of MBP adsorption onto the bilayers are detected and the results are very similar to bare bilayers (Fig. 5*A*). However, when the separation distance between two bilayers is small (~2 nm), a "depletion zone" exists in which η is slightly smaller than the bulk viscosity η_b and is similar to water's viscosity η_w, which is a clear effect from MBP in solution that did not adsorb to the bilayer surfaces. The existence of a depletion zone in nonadsorbing polymeric solutions already was shown by Kuhl et al. (40). When C is higher than 2.9 ng/mL (Fig. 5*C*), completely different rheological properties related to MBP adsorption are observed: (*i*) the hydrodynamic thickness Δ_H is shifted outward about ~5.5 nm for each surface; (*ii*) the thickness of the diffusive MBP layer is estimated to be D ~21 nm; (*iii*) when the two diffusive MBP layers overlap, the effective viscosity of the MBP film increases up to two to threee times of η_b.

The trends are similar for normal bilayers (Fig. S1); however, D_{MBP}, Δ_H, and the diffuse MBP layer thickness are ~2.5, 1.3 and 4 nm, respectively, which are smaller compared with those of EAE bilayers. The smaller values of the above three parameters obtained for normal bilayers compared with EAE bilayers indicate that MBP is adsorbed in a more compact manner on normal bilayers (without swelling and a thick gel-like layer formation), which is consistent with the higher adhesion of normal bilayers.

Selective Distribution of MBP on the Lipid Membrane. Several proteins are known to adhere selectively to lipid domains of biological membranes (41); however, the role of lipid domains in the distribution of MBP still is not established. Previous studies (8, 10) conducted with fluorescence microscopy showed the absence of micrometer-sized domains at a surface pressure, Π, of ~30 mN/m. However, because of the resolution limit of the fluorescence microscope, submicron- or nano-sized domains still may exist.

Fig. 6 shows the topography of the EAE myelin lipid bilayers as a function of MBP concentration imaged with an atomic force microscope in aqueous solution. Bilayers without MBP (Fig. 6*A*) had a thickness of ~5 nm, which was consistent with the SFA measurements. Also, noncircular nano-sized domains (area fraction of 8%) were observed and were ~0.5 nm thinner than the surrounding bilayer, indicating that these domains were in a liquid-disordered phase (L_d) and the surrounding bilayer was in a liquid-ordered phase (L_o).

After injecting a low concentration of MBP (Fig. 6*A*, C ~2.5 ng/mL), no changes in the bilayer structure were observed compared with the bare bilayer. However, when C was increased to 125 ng/mL (Fig. 6*B*), MBP adsorbed selectively only to L_d lipid domains. MBP-bound lipid domains became ~2 nm thicker than the (MBP-free) L_o phase, indicating an MBP thickness of ~3 nm, which is consistent with the SFA measurements and previous studies (9, 14, 42). Also, the area fraction of bilayer holes (which we used to confirm the bilayer thickness; see Fig. S2 for larger AFM images) decreased after the MBP adsorption (from 14% to 12%), which provides evidence of bilayer expansion caused by partial penetration of MBP into the upper leaflet of the bilayer due to the hydrophobic attraction between the hydrophobic moieties of MBP and hydrocarbon chains of the myelin bilayer. The selective adsorption of MBP to the L_d phase should be a result of the hydrophobic interaction, because the lipids in the L_d phase have a greater molecular area compared with those in the L_o phase, i.e., more hydrophobic residues are exposed. The normal model bilayers did not show significant differences in terms of selective MBP adsorption; however, they exhibited a higher area fraction of L_d+MBP phase (8.4%) compared with EAE lipid bilayers (5.5%) (Fig. S3).

At bulk MBP concentrations up to 375 ng/mL (Fig. 6*C*), the MBP adsorbs unselectively to both the L_d and L_o phases, and the thickness difference between the two phases becomes very small (< 0.5 nm). In addition, MBP adsorbs to bilayer holes that cause the depth of the holes in the lipid bilayer to be smaller (2 nm). The nonselective adsorption of MBP to the bilayer surface causes MBP to cover the whole bilayer surface (possibly as a multilayer), forming a gel-like film, as found by viscosity measurements. The gel-like structure of MBP, which possibly is induced by the cohesion between β-sheet regimes of MBP (11, 23), may alter the structure and orientation of MBP. The altered structure of MBP might not be optimal for the high interbilayer adhesion force in myelin. This result is consistent with the SFA results showing a decrease in adhesion after an excessive amount of MBP for both normal and EAE bilayers (Fig. 3).

Discussion

MBP Structure and Adsorption Mechanism on Bilayers. The results provide qualitative and quantitative information regarding not only the structure of adsorbed MBP but also the mechanism of how MBP adsorbs to myelin bilayer surfaces. Based on these results and previous studies (14, 42, 43) of normal myelin bilayers, MBP should be forming a thin yet compact structure (Fig. 1) with a thickness of ~3 nm, holding two opposing bilayers together via electrostatic and hydrophobic interactions. Here we find that between two EAE bilayers, the compact structure of MBP is disturbed and forms a swollen gel-like structure (~6–7 nm thickness) and a thick diffuse MBP layer (~21 nm) with a hydrodynamic thickness ~5.5 nm, as confirmed by normal force (Fig. 2) and film viscosity (Fig. 5) measurements. The thick gel-like MBP layer causes a significant decrease in the adhesion force (4, 6, 9), which might be one of the causes, at a molecular level, of bilayer degradation during the progression of demyelinating diseases.

The fact that MBP does not adsorb below a certain bulk concentration C_{crit}, whereas rapid adsorption of MBP occurs above C_{crit}, is consistent with cooperative adsorption. The cooperative adsorption of MBP is involved closely in protein–protein and protein–lipid/lipid domain interactions, which might be an effective way for the MBP to bind to myelin bilayers, resulting in a(n) (optimum) high adhesion force.

Role of Lipid Domains in the Myelin Membrane. The existence and functions of lipid domains in myelin membranes already were shown in many studies (8–10, 44). Normal and EAE myelin lipid monolayers have different lipid domain sizes and distributions at the same temperature and surface pressure (8, 10) that are attributed to small differences in lipid compositions (Table 1). These differences in lipid composition also give rise to different membrane fluidities while the lipid charge density remains similar. The measured differences in adhesion characteristics (Fig. 3) and MBP coverage (Fig. 4) between normal and EAE bilayers result from differences in membrane fluidity and/or lipid domain distribution. Sphingomyelin, known to be critical for the formation of liquid-ordered phases in multicomponent lipid membranes (41), is up to three times more abundant in normal compared with EAE myelin bilayers. Cholesterol also is known to contribute to lipid domain formation (41) and affects the fluidity of membranes (45), and EAE myelin contains more cholesterol than normal myelin (Table 1).

Because the charge density between normal and EAE bilayers is similar, all the differences between normal and EAE bilayers are

the result of lipid fluidity and/or lipid domains. Without MBP between bilayers, the force profiles show little difference between normal and EAE bilayers. Above C_{crit} of MBP, the force profiles show significant discrimination between normal and EAE bilayers: with increasing C, the force profile of normal bilayers shows an increase in the adhesion force while the bilayers maintain a compact structure, whereas the EAE bilayers show little increase in the adhesion force with significant swelling of the system.

AFM results (Fig. 6) show that MBP binds selectively to the L_d phase of lipid bilayers up to a certain bulk MBP concentration. Thus, it may be concluded that although membrane fluidity and lipid domains have minimal effect on the adhesive properties between supported lipid bilayers, lipid domains modify the mechanism of MBP adsorption (e.g., amount, structure, and orientation) onto the model myelin bilayers that directly affect the intermembrane adhesion mediated by MBP.

Implications for Demyelinating Diseases. The forces between bilayers of myelin with phase-separated lipid domains and an inhomogeneous protein distribution are fundamentally different from those between single-phase and homogeneous bilayers. These inhomogeneities can dramatically amplify the effect of even small changes in the lipid composition or protein isoform (20), resulting in large changes in bilayer adhesion (7, 15) that may cause the myelin sheath to unravel. Lipid domains within lipid bilayers are known to be correlated with bilayer–bilayer interactions (46) and may play important roles in adhesion (47), intermembrane spacing (48), and permeability (49). Lipid domains also are thought to act as platforms on which proteins can adsorb selectively (50). Accordingly, any difference in lipid domain organization within myelin bilayers most likely will alter the MBP adsorption properties, as well as intermembrane adhesion and spacing, and will have a direct impact on the stability of the myelin structure. When the stability of the membrane structure is disturbed, the myelin might be more susceptible to attack by the immune system and possibly progress to demyelinating diseases such as MS.

The primary cause of demyelinating diseases (such as MS) still is under debate, as is the molecular mechanism of intermembrane (de-)stabilization. Here, we focused on the effects of lipid composition and MBP concentration on intermembrane adhesion. With normal model myelin bilayers, we observed a compact protein layer with a thin MBP film, resulting in high intermembrane adhesion, whereas with EAE bilayers, swelling and a decrease in adhesion were observed. Swelling of the myelin membrane increases the dielectric constant between the neural core (e.g., axon) and the medium surrounding the neural cell, which reduces electric conduction through the axon and weakens or deteriorates the signal's transmission through the nervous system. The swelling and loss of adhesion might contribute to the disruption of myelin structure during the progression of demyelinating diseases (such as MS), from which one might infer that the molecular indication of membrane swelling and loss of adhesion may originate from an alteration of lipid composition and MBP concentration.

Materials and Methods

Normal and EAE Cytoplasmic Model Myelin. A previous study (6) using NMR and HPLC techniques identified the lipid composition of white matter from normal and diseased marmosets after induction of EAE. With the distribution of lipids in myelin determined by Inouye and Kirschner (1, 24), lipid compositions of both normal and EAE cytoplasmic leaflets were calculated (Table 1).

To mimic the cytoplasmic myelin leaflet, the following porcine brain-extracted lipids were purchased from Avanti Polar Lipids, stored in chloroform, and kept in a deep freezer (−50 °C) until used: phosphatidylserine (porcine brain PS^{-}), sphingomyelin (porcine brain $SM^{+/-}$), phosphatidylcholine (porcine brain $PC^{+/-}$), phosphatidylethanolamine (porcine brain $PE^{+/-}$), and cholesterol (ovine wool). The major fatty acid chain lengths of the PC, PE, and PS are 16:0, 18:0, 18:1, and 20:4. Dipalmitoylphosphatidylethanolamine (DPPE), sodium nitrate (purity ≥99.0%), and morpholinepropanesulfonic acid (Mops) sodium salt (purity ≥99.5%) were purchased from Sigma–Aldrich. To disperse the lipids, the following solvents were purchased from Sigma–Aldrich: chloroform (CHROMASOLV Plus for HPLC, purity ≥99.9%), hexane (RegentPlus, purity ≥99.0%), ethanol (200 proof, HPLC/spectrophotometric grade), and methanol (CHROMASOLV Plus for HPLC, purity ≥99.9%). MBP was isolated from bovine brain white matter (51) and kept in a deep freezer (−50 °C) until use.

Supported Bilayer Preparation. Freshly cleaved and back-silvered atomically smooth mica sheets were glued onto two cylindrical glass disks with curvature radii of 2 cm. Lipid bilayers were deposited onto the mica using the Langmuir–Blodgett deposition technique (25). For the first supporting monolayer, 100 μL of 1 mg/mL DPPE solution [3:1 (vol/vol) chloroform/methanol] was spread onto Milli-Q water (Millipore) and deposited at a surface pressure of 35 mN/m (molecular area of ∼43 $Å^2$). For the second layer, normal and EAE myelin lipid solutions were prepared (see the lipid composition in Table 1) in dispersed form in the 11:5:4 (vol/vol) hexane/chloroform/ethanol solvent mixtures. The second layer was deposited onto the DPPE-deposited mica substrates at a surface pressure of 30 mN/m (molecular area of ∼50–52 $Å^2$) with a subphase of sodium nitrate buffer (150 mM sodium nitrate/10 mM Mops sodium salt, pH 7.4). The bilayer-deposited samples were transferred immediately to the SFA chamber (without being exposed to air) prefilled with degassed saturated lipid solution (sodium nitrate buffer in contact with lipid crystals for 12 h, and degassed for 2 h before the experiment).

SFA Experiments. The SFA 2000 (26) was used in this study for the force measurements. Bilayer-deposited disks were installed in the SFA chamber in a cross-cylindrical geometry, which at small separation distances, is equivalent to a sphere-on-flat geometry. The separation distance between two surfaces is measured using optical interferometry (52), and the force between two surfaces can be calculated from the deflection of a double-cantilever spring of known spring constant that holds the lower disk holder. For the force–distance measurements, the surfaces approach each other with a speed of 0.5–1.0 nm/s, which is expected to be slow enough to maintain a quasi-equilibrium state at all times. To measure film viscosity (38, 39), a piezoelectric crystal was used to oscillate the upper surface relative to the lower surface at an applied amplitude A_0 by applying an ac voltage (15 V, 0.5 Hz, square wave for A_0 and sine wave for the relative amplitude A) to the piezoelectric crystal. While oscillating, the surfaces slowly are brought closer together in a stepwise manner while measuring the relative amplitude A with varying D.

MBP solution (dissolved in sodium nitrate solution) was prefiltered with an Anotop10 0.1-μm filter (Whatman) and injected into the SFA chamber in a stepwise manner after the two bilayers were separated far from each other ($D > 1$ mm). After each injection, the system was equilibrated for 0.5 h, allowing sufficient time for MBP to adsorb to the model myelin bilayers.

AFM Experiments. Images were acquired with an MFP-3D-Bio AFM (Asylum Research) using an MSNL probe (Bruker) with a spring constant of 0.1 ± 0.05 $N{\cdot}m^{-1}$. Scanning was performed in tapping mode at room temperature (22 ± 1 °C) in lipid-saturated sodium nitrate buffer (150 mM sodium nitrate/10 mM Mops sodium salt, pH 7.4). The EAE myelin bilayers were prepared as described above and covered with 4 mL of sodium nitrate buffer in a reservoir. MBP concentration was increased from 0 to 375 ng/mL by stepwise injection of MBP solution (prepared as in SFA experiments) into the reservoir. The sample was equilibrated for 30 min after each injection.

ACKNOWLEDGMENTS. This work was supported by National Institutes of Health Grant R01 GM076709. X.B. and Y.K. are grateful for the financial support of the Santa Barbara Foundation through the Otis Williams Fellowship. J.M.B. thanks Canadian Institutes of Health Research Grant MOP 86483.

1. Inouye H, Kirschner DA (1988) Membrane interactions in nerve myelin. I. Determination of surface charge from effects of pH and ionic strength on period. *Biophys J* 53(2):235–245.
2. Morell P (1984) *Myelin* (Plenum, New York), 2nd Ed.
3. Martenson R (1992) *Myelin: Biology and Chemistry* (CRC, Boca Raton, FL).
4. Genain CP, Cannella B, Hauser SL, Raine CS (1999) Identification of autoantibodies associated with myelin damage in multiple sclerosis. *Nat Med* 5(2):170–175.
5. Hafler DA (2004) Multiple sclerosis. *J Clin Invest* 113(6):788–794.
6. Ohler B, et al. (2004) Role of lipid interactions in autoimmune demyelination. *Biochim Biophys Acta* 1688(1):10–17.

7. Banquy X, Kristiansen K, Lee DW, Israelachvili JN (2012) Adhesion and hemifusion of cytoplasmic myelin lipid membranes are highly dependent on the lipid composition. *Biochim Biophys Acta* 1818(3):402–410.
8. Min Y, et al. (2011) Critical and off-critical miscibility transitions in model extracellular and cytoplasmic myelin lipid monolayers. *Biophys J* 100(6):1490–1498.
9. Min Y, et al. (2009) Interaction forces and adhesion of supported myelin lipid bilayers modulated by myelin basic protein. *Proc Natl Acad Sci USA* 106(9):3154–3159.
10. Lee DW, et al. (2011) Relating domain size distribution to line tension and molecular dipole density in model cytoplasmic myelin lipid monolayers. *Proc Natl Acad Sci USA* 108(23):9425–9430.
11. Sedzik J, Kirschner DA (1992) Is myelin basic protein crystallizable? *Neurochem Res* 17(2):157–166.
12. Boggs JM (2006) Myelin basic protein: A multifunctional protein. *Cell Mol Life Sci* 63(17):1945–1961.
13. Harauz G, Ladizhansky V, Boggs JM (2009) Structural polymorphism and multifunctionality of myelin basic protein. *Biochemistry* 48(34):8094–8104.
14. Beniac DR, et al. (1997) Three-dimensional structure of myelin basic protein. I. Reconstruction via angular reconstitution of randomly oriented single particles. *J Biol Chem* 272(7):4261–4268.
15. Hu Y, et al. (2004) Synergistic interactions of lipids and myelin basic protein. *Proc Natl Acad Sci USA* 101(37):13466–13471.
16. MacNaughtan W, Snook KA, Caspi E, Franks NP (1985) An X-ray diffraction analysis of oriented lipid multilayers containing basic proteins. *Biochim Biophys Acta* 818(2): 132–148.
17. Mueller H, Butt HJ, Bamberg E (1999) Force measurements on myelin basic protein adsorbed to mica and lipid bilayer surfaces done with the atomic force microscope. *Biophys J* 76(2):1072–1079.
18. Wheeler D, Bandaru VVR, Calabresi PA, Nath A, Haughey NJ (2008) A defect of sphingolipid metabolism modifies the properties of normal appearing white matter in multiple sclerosis. *Brain* 131(Pt 11):3092–3102.
19. Jo EJ, Boggs JM (1995) Aggregation of acidic lipid vesicles by myelin basic protein: Dependence on potassium concentration. *Biochemistry* 34(41):13705–13716.
20. Husted C (2006) Structural insight into the role of myelin basic protein in multiple sclerosis. *Proc Natl Acad Sci USA* 103(12):4339–4340.
21. Musse AA, Boggs JM, Harauz G (2006) Deimination of membrane-bound myelin basic protein in multiple sclerosis exposes an immunodominant epitope. *Proc Natl Acad Sci USA* 103(12):4422–4427.
22. Aggarwal S, et al. (2013) Myelin membrane assembly is driven by a phase transition of myelin basic proteins into a cohesive protein meshwork. *PLoS Biol* 11(6):e1001577.
23. Kattnig DR, Bund T, Boggs JM, Harauz G, Hinderberger D (2012) Lateral self-assembly of 18.5-kDa myelin basic protein (MBP) charge component-C1 on membranes. *Biochim Biophys Acta* 1818(11):2636–2647.
24. Inouye H, Kirschner DA (1988) Membrane interactions in nerve myelin: II. Determination of surface charge from biochemical data. *Biophys J* 53(2):247–260.
25. Zasadzinski JA, Viswanathan R, Madsen L, Garnaes J, Schwartz DK (1994) Langmuir-Blodgett films. *Science* 263(5154):1726–1733.
26. Israelachvili J, et al. (2010) Recent advances in the surface forces apparatus (SFA) technique. *Rep Prog Phys* 73(3):036601.
27. Israelachvili J (1994) Self-assembly in two dimensions—surface micelles and domain formation in monolayers. *Langmuir* 10(10):3774–3781.
28. Israelachvili JN (2011) *Intermolecular and Surface Forces* (Academic, London), 3rd Ed.
29. Johnson KL, Kendall K, Roberts AD (1971) Surface energy and contact of elastic solids. *Proc R Soc Lond A Math Phys Sci* 324(1558):301–313.
30. Haas H, et al. (2004) Small angle x-ray scattering from lipid-bound myelin basic protein in solution. *Biophys J* 86(1 Pt 1):455–460.
31. Ridsdale RA, Beniac DR, Tompkins TA, Moscarello MA, Harauz G (1997) Three-dimensional structure of myelin basic protein. II. Molecular modeling and considerations of predicted structures in multiple sclerosis. *J Biol Chem* 272(7):4269–4275.
32. Tadmor R, Chen NH, Israelachvili JN (2003) Thickness and refractive index measurements using multiple beam interference fringes (FECO). *J Colloid Interface Sci* 264(2): 548–553.
33. Israelachvili JN, Sammut RA, Snyder AW (1976) Birefringence and dichroism of photoreceptors. *Vision Res* 16(1):47–52.
34. Barer R, Tkaczyk S (1954) Refractive index of concentrated protein solutions. *Nature* 173(4409):821–822.
35. Fisk AA (1950) The thicknesses of hemoglobin and bovine serum albumin molecules as unimolecular layers adsorbed onto films of barium stearate. *Proc Natl Acad Sci USA* 36(10):518–523.
36. Raviv U, et al. (2002) Properties and interactions of physigrafted end-functionalized poly(ethylene glycol) layers. *Langmuir* 18(20):7482–7495.
37. Smith R (1982) Self-association of myelin basic protein: Enhancement by detergents and lipids. *Biochemistry* 21(11):2697–2701.
38. Israelachvili JN (1986) Measurement of the viscosity of liquids in very thin-films. *J Colloid Interface Sci* 110(1):263–271.
39. Israelachvili JN (1986) Measurements of the viscosity of thin fluid films between two surfaces with and without adsorbed polymers. *Colloid Polym Sci* 264(12):1060–1065.
40. Kuhl TL, Berman AD, Hui SW, Israelachvili JN (1998) Direct measurement of depletion attraction and thin film viscosity between lipid bilayers in aqueous polyethylene glycol solutions. *Macromolecules* 31(23):8250–8257.
41. Simons K, Ehehalt R (2002) Cholesterol, lipid rafts, and disease. *J Clin Invest* 110(5): 597–603.
42. Keniry MA, Smith R (1979) Circular dichroic analysis of the secondary structure of myelin basic protein and derived peptides bound to detergents and to lipid vesicles. *Biochim Biophys Acta* 578(2):381–391.
43. Ahmed MAM, Bamm VV, Harauz G, Ladizhansky V (2010) Solid-state NMR spectroscopy of membrane-associated myelin basic protein—conformation and dynamics of an immunodominant epitope. *Biophys J* 99(4):1247–1255.
44. Debruin LS, Harauz G (2007) White matter rafting—membrane microdomains in myelin. *Neurochem Res* 32(2):213–228.
45. Cooper RA (1978) Influence of increased membrane cholesterol on membrane fluidity and cell function in human red blood cells. *J Supramol Struct* 8(4):413–430.
46. Tayebi L, et al. (2012) Long-range interlayer alignment of intralayer domains in stacked lipid bilayers. *Nat Mater* 11(12):1074–1080.
47. Nusrat A, et al. (2000) Tight junctions are membrane microdomains. *J Cell Sci* 113 (Pt 10):1771–1781.
48. Kaizuka Y, Groves JT (2004) Structure and dynamics of supported intermembrane junctions. *Biophys J* 86(2):905–912.
49. Rawicz W, Smith BA, McIntosh TJ, Simon SA, Evans E (2008) Elasticity, strength, and water permeability of bilayers that contain raft microdomain-forming lipids. *Biophys J* 94(12):4725–4736.
50. Simons K, Ikonen E (1997) Functional rafts in cell membranes. *Nature* 387(6633): 569–572.
51. Cheifetz S, Moscarello MA (1985) Effect of bovine basic protein charge microheterogeneity on protein-induced aggregation of unilamellar vesicles containing a mixture of acidic and neutral phospholipids. *Biochemistry* 24(8):1909–1914.
52. Israelachvili J (1973) Thin-film studies using multiple-beam interferometry. *J Colloid Interface Sci* 44(2):259–272.